OVERVIEW ON W7-AS RESULTS WITH RELEVANCE FOR WENDELSTEIN 7-X AND THE LOW-SHEAR STELLARATOR LINE

WAGNER, F., ANTON, M., BALDZUHN, J., BLEUEL, J., BRAKEL, R., BURHENN, R., CATTANEI, G., ENDLER, M., ERCKMANN, V., FENG, Y., FIEDLER, S., GEIGER, J., GEIST, T., GIANNONE, L., GRIGULL, P., HARTFUSS, H.-J., HARTMANN, D., HERRE, G., HIRSCH, M., HOLZHAUER, E., JÄNICKE, R., KICK, M., KISSLINGER, J., KOPONEN, J., KÜHNER, G., LAQUA, H.P., MAASSBERG, H., SARDEI, F., STROTH, U., WELLER, A., ZOLETNIK, S., CHATENET, J.H., DORST, D., ELSNER, A., GÖRNER, C., HACKER, H., KARGER, F., KNAUER, J., KÖNIG, R., LAQUA, H., MCCORMICK, K., NIEDERMEYER, NÜHRENBERG, C., OTT, W., PENNINGSFELD, F.-P., SALAT, A., SCHNEIDER, F., THEIMER, G., WALTER, H., WENDLAND, C., WERNER, A., WÜRSCHING, E., ZEILER, P.

Max-Planck-Institut für Plasmaphysik, EURATOM Association, Garching, Germany

Abstract

The Wendelstein stellarator programme of Garching has developed low shear stellarators with successively optimised designs to remove the intrinsic deficiencies of this 3D concept. W7-X, presently under construction, is in internal terminology a fully optimised stellarator. W7-AS, the presently operated device, is a partly optimised stellarator. The optimisation of stellarators aims at improved neoclassical confinement in the long mean free path regime and improved equilibrium and stability properties. In this report, we address equilibrium, stability, turbulent and collisional energy confinement aspects (role of magnetic shear, role of the radial electric field, low and improved confinement regimes), particle transport, transport and turbulence at the plasma edge, high density operation, ECRH (OXB scheme) and ICRF heating and the deve-lopment of the island divertor for exhaust. The maximal parameters achieved in W7-AS (at dif-ferent discharge types) are: T_e = 5.8 keV, T_i = 1.5 keV, $n_e = 3 \times 10^{20}$ m^{-3}, $\langle\beta\rangle$ = 2%, τ_E = 50 ms.

The W7-X concept:

The stellarator Wendelstein 7-X (W7-X, presently under construction in Greifswald, Mecklenburg-Vorpommern, Germany) is optimised based on the concept of quasi-isodynamicity /1/. A truly isodynamic confinement geometry has poloidal symmetry with the consequence of plasma flows on a flux surface only, without neoclassical radial fluxes. In order to utilise this concept in a toroidally closed system, a specific geometry is necessary. Straight and helical sectors alternate forming - viewed from above - a pentagon in the case of W7-X. The magnetic field is increased at the corners of the pentagon to restrict reflected particles to the straight sectors where their banana orbits rotate poloidally. By this means radial neoclassical fluxes at the low level of that of symmetric systems can be achieved. In order to guarantee the high-β to be only weakly dependent on β (resistive ballooning is expected to limit W7-X to 5%), pressure driven parallel currents must also be minimised. The concept of quasi- isodynamicity allows $\langle j_{\|}^2\rangle/\langle j_{\perp}^2\rangle$, which is $2/\iota^2$ for a classical stellarator, to be reduced to $0.32/\iota^2$ ($\iota = \iota/2\pi$) for W7-X, and the bootstrap current to be simultaneously minimised. To reduce $\langle j_{\|}^2\rangle$, the plasma cross-sections are strongly elongated at the corners ($\kappa \approx 3.6$); bootstrap current could be minimised in W7-X (unlike in quasi-helical or quasi-toroidal systems - in the latter case a strong bootstrap current is actually desired) by appropriately adjusted toroidal and helical curvatures. Thus, the properties of the optimised design are only weakly dependent on β. The rotational transform ι of W7-X is selected around $\iota(a) = 1$ ($0.8 \le \iota(a) \le 1.2$) with a small variation between core and edge ($0.8 \le \iota(a) \le 1$ or $1 \le \iota(a) \le 1.25$); low shear promises good confinement as long as low order m/n field perturbations are avoided. In order to also minimise high m/n turbulence, limited magnetic shear is provided to

the extent that low order rationals are still excluded. An edge separatrix can be formed via a chain of edge islands (5/5 or alternatively 5/6) which are radially extended because of low shear and consequently are expected to effectively divert the fluxes from the plasma and to establish the magnetic part of an island divertor.

The W7-AS device:

W7-AS has the form of a pentagon and its field structure is partly optimised ($\langle j_{\parallel}^2\rangle/\langle j_{\perp}^2\rangle$ = 0.85 $\iota(a)^2$) /2/. The field system is composed of modular coils ($\iota(a) = 0.4$); toroidal field coils allow changes of $\iota(a)$, vertical field coils allow to vary the radial plasma position; W7-AS is also equipped with an OH system e.g. to compensate the bootstrap current. In addition, the magnetic field strength in the corners of the pentagon can be varied (variation of mirror ratio). The bootstrap current is tokamak-like and increases $\iota(a)$; generally, operation is such that a superimposed inductive current cancels this increase of the edge rotational transform $\iota(a)$ to maintain the pre-set value. Shear can be varied with OH current and by ECCD. The vertical field allows changes of the magnetic well and thus modifies stability properties. In addition, it allows changes of the plasma wall interaction with 5×2 graphite tiles mounted symmetrically at the inboard walls.

Equilibrium properties:

The optimisation of W7-AS has been demonstrated by indirect measurement of the parallel currents $\langle j_{\parallel}^2\rangle$ which were found to be reduced as expected /3/ and by the demonstration of reduced Shafranov shift in high β equilibria in comparison to a classical l = 2 stellarator /4/. Maximum $\langle\beta\rangle$-values close to 2% have been reached at W7-AS. This limitation is due to restricted heating power at given radiation losses. High β operation is carried out at low field of ≤ 1.25 T and at high density. Under these conditions, orbit losses are predicted for energetic particles injected by the counter beam line /5/. The increase in β with NBI is found to be mainly due to the co-beams. The additional increment in β achieved with the counter beams is small. The high-β programme on W7-AS will be continued with reversing the counter injector into co-direction. Under these conditions it is expected that β is limited by resistive interchange /6/.

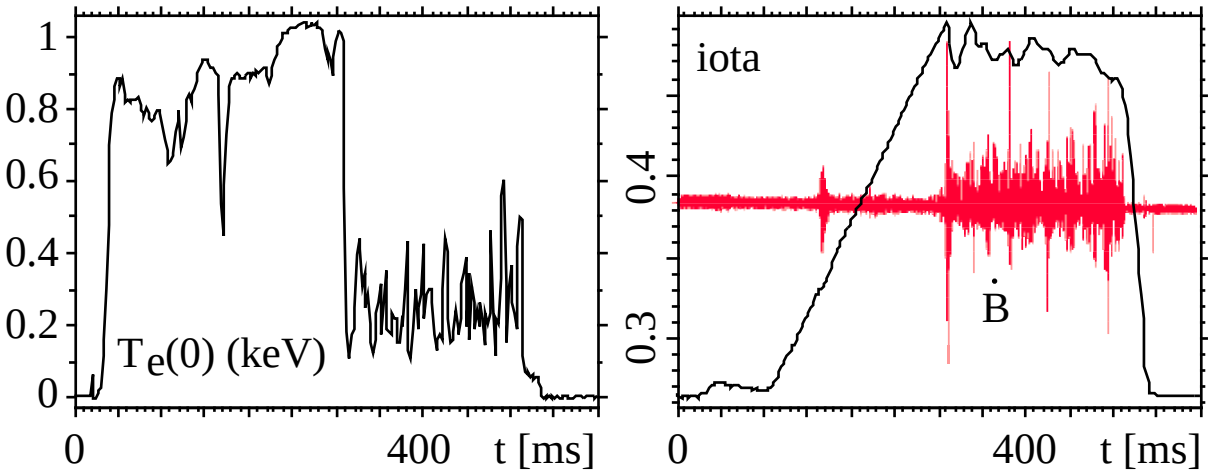

Fig. 1. Development of a discharge with rising OH current. Left: Central electron temperature; right: rise of external rotational transform ι_a and Mirnov signal.

Stability properties:

The high-β plasmas of W7-AS are rather quiescent, and reach stationary phases till the heating has been turned off /7/. No violent MHD processes occur in the high- β phase. With a low-order rational in the plasma core, a pressure driven mode may appear which rotates in

electron drift direction with a few kHz and which does not reduce the energy content of the plasma. With plasma current - either bootstrap current, or induced current by OH or ECCD /8/ - current driven tearing modes can appear due to resonances. Their impact on the plasma depends on the current level. Although the plasma does not disrupt, the current induced formation of tearing mode islands causes the irreversible loss of a major part of the energy content /9/. A current induced rise in ι(a) by $\Delta\iota \approx 0.2$ is sufficient, if ι(a) = 0.5 is reached to expel 80% of the energy content. Figure 1 shows the discharge development in such a scenario. Plotted is the central temperature, the variation of ι_a by the plasma current and finally the development of unstable conditions seen in the Mirnov signals.

The most conspicuous MHD feature of W7-AS are global Alfvén eigenmodes (GAE) which are driven by that part of the fast particle spectrum which is in resonance /10/. In case of side-band excitation (m±1), particle velocities down to $v_A/10$ can contribute. GAEs appear typically in the absence of a rational ι in the plasma and in the low shear case of W7-AS their frequency resides closely below the corresponding continuum band. The frequency varies with density, isotope mass and field in the expected form. The GAE modes generally saturate at a level up to $\delta B/B \approx 10^{-4}$ there is no evidence, at present, that they limit the NBI heating efficiency (locally or globally). With shear (via induced current), the GAE activity changes into TAE modes which are more localised (at the gap) and are characterised by a larger poloidal harmonic content. The mode pattern depends on ι and a large variety is observed - cases up to m = 9 and cases with a node in the radial eigenfunction are observed. For both the GAE and the TAE activity, the eigenfunctions are well described by a three-dimensional MHD code (CAS 3D /11/) and by a gyrofluid model /12/.

Confinement and the role of shear:

Low vacuum field shear in the Wendelstein line is a design characteristic. The idea behind low shear is that low-order resonances arising from the mode spectrum of the magnetic field as well as from external field perturbations should be avoided as they reduce by the development of magnetic islands - as originally thought. The most obvious experimental evidence is that, in the accessible ι-range of W7-AS, good confinement is established in the vicinity of ι(a) = 1/2 and 1/3 where larger ι-intervals free of resonances occur. (Empirically, it is found that resonances beyond m=20 have no influence.). There is ample experimental evidence which demonstrates the sensitivity of confinement on ι(a) (see Fig. 2, left side). At low shear, confinement can be „good“ but, without further means, it is at the L-mode level (e.g. in the iota window $0.50 \leq \iota(a) \leq 0.53$. Outside this range, the confinement is at a sub-L-mode level. As described below, confinement can be increased to the H-mode level in the favourable ι-windows.

The shear studies of W7-AS are of general interest because of the low central magnetic shear obviously required for advanced tokamak scenarios and because different theoretical concepts exist predicting different dependencies of turbulent transport on shear. The studies are carried out for $T_e/T_i >> 1$ (ECRF heating) and only the response of electron transport on shear is investigated. The current necessary to introduce strong shear in W7-AS is too low ($I_p \leq 30$ kA) to affect the power balance /11/.

The impact of ι and shear S can be separated at low shear ($I_p < 5$kA, $\Delta\,\iota(a) = 0.007 I_p/$kA). Good confinement develops if specifically the plasma periphery remains free of resonances. Little shear is tolerable in this case. On the contrary, if the edge value, ι(a), is selected such that rational ι-values (m < 20) intersperse the plasma outer range, the temperature gradient is flat and confinement is degraded in case of insufficient shear. Good confinement is possible even in the presence of resonances, if sufficient shear is established. With strong shear ($I_p \approx \pm 25$ kA) - and the sign of S does not matter - the confinement is good and loses its subtle dependencies on iota (see Fig. 2, left side) /13, 14/. The shear where ι loses its impact is about $S \approx 1$ m^{-1}. A rather sensitive situation is established at low shear. Little shear can degrade good confinement or improve bad confinement depending on the preselected value of ι(a). Under marginal conditions, good confinement can be transformed into degraded confinement (sub-L-mode level) if the

plasma current (e.g. self-induced) moves ι(a) into the range with resonances. Also the opposite has been observed.

The impact of resonances on transport can be modelled /15/ by a composition of the electron heat diffusivity from three components: the neoclassical χ_{neo}, the anomalous one χ_{an}, which describes the good confinement (L-mode level) and an additional one $\Sigma\chi_{nm}$ which represents the contribution of the resonances. The view is that resonances do not necessarily cause islands, which short-circuit a small radial range, but rather that it gives rise to locally enhanced turbulence. The χ_{nm} term is parameterized by an amplitude a_{nm}, a radial range of effectiveness and a damping factor which itself depends on shear. There are three fit-parameters which are determined from the confinement results in experimental scans which allowed χ_{nm} to be varied. Figure 2 compares the experimentally measured variation of the energy content W with ι(a) at different plasma currents (shear values) with the modelling results. The existence of enhanced turbulence at the location of a resonance has not yet been demonstrated. Microwave scattering shows, however, that the integral density fluctuation level is enhanced under degraded confinement in the radial range of the resonances.

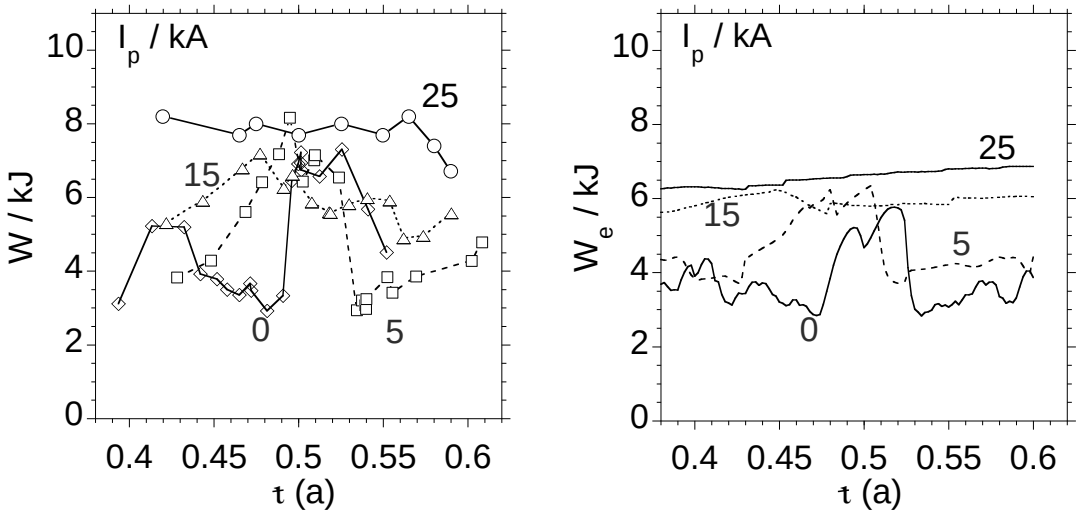

Fig. 2 shows the experimental variation of the energy content W with ι_a; parameter is the plasma current I_p; the right side shows the modelled dependence of the electron energy content W_e.

Neoclassical core transport:

In cases of improved confinement, the core electron temperature rises and because of the strong T_e-dependence of Q_{neo} ($\approx T_e^{9/2}$ (without E_r-field)), the core confinement becomes neoclassical. The better confinement is, the more extended is the neoclassical core /16/.

In those cases where a separate analysis is possible, the ion transport in the plasma core is found to be at the neoclassical level. Under good confinement conditions at high electron temperature, the electron core transport can also be neoclassical. With established electric field, the highest ion- and electron temperatures are measured - under different discharge conditions, however: 1.5 keV and 5.8 keV, respectively. The presence of E_r reduces the heat diffusivities by up to one order of magnitude from the expected neoclassical level without field.

The neoclassical fluxes in stellarators depend explicitly on the radial electric field which itself is determined by the balance of the particle fluxes. The radial electric field represents a thermodynamic force and drives particle flux Γ ($\approx D_{11} E_r/T_e$) whereas the diffusivities (D_{11},D_{12}) depend themselves on E_r. The non-linear relation allows different branches of stable transport equilibria which depend operationally on T_e/T_i /17/. The agreement between the measured radial electric field and the one computed on the basis of neoclassical transport even for turbulent

plasma conditions points, as in other cases, to the intrinsic ambipolarity of the prevailing electrostatic turbulence. The highest ion temperatures are obtained with NBI when $T_e \approx T_i$. In this case the ion root develops and is characterised by a negative electric field. The highest electron temperature develops with ECRH when $T_e >> T_i$. Here the electron root is establshed in the plasma core whereas the plasma periphery remains at the ion root. Detailed analysis has shown that the electron root cannot develop in W7-AS exclusively on the basis of thermal fluxes rather the loss of non-thermal electrons energised by ECRH contributes to the ambipolarity condition /18/. In the experiment the bifurcation point between the two roots can be selected and the plasma responds at this setting with unstable behaviour (Figure 3 shows the consequence of a dithering behaviour of the neo-classical ambipolarity condition on T_e): T_e of the core plasma oscillates between a state with low electric field (ion root) and one with high field (electron root) with E_r improved neoclassical confinement. The plasma periphery remains passively at the ion root.

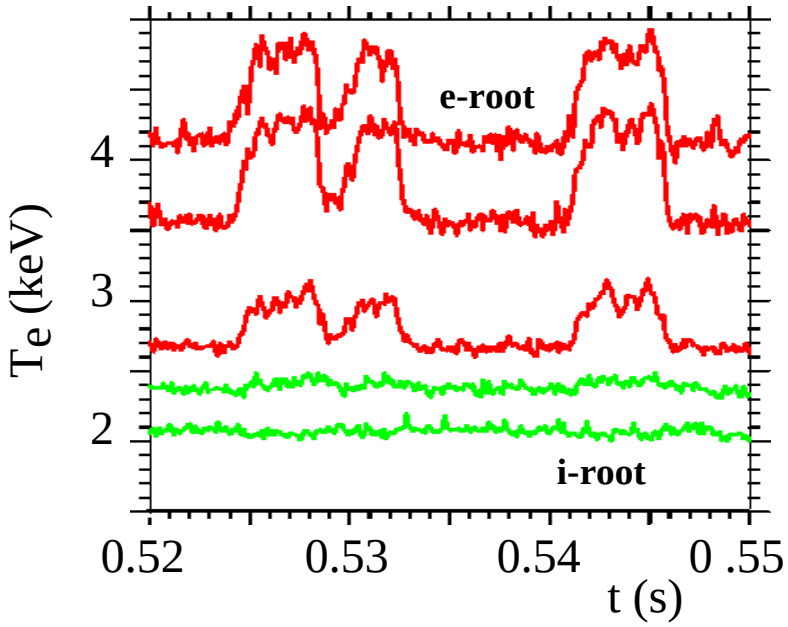

Fig. 3. Plotted is the electron temperature at different radii versus time for a marginal case where the plasma core switches between the electron- (highly positive electric field) and ion root (low positive field). The periphery remains at the ion root.

Global confinement and improved regimes:

The W7-AS energy confinement data are part of the International Stellarator Scaling ISS95 /19/. Data are selected only from the iota ranges around 0.334 and 0.53 where confinement is good at the L-mode level (the turbulent plasma periphery determines τ_E also in cases with neo-classical core). It is interesting that the τ_E values of W7-AS are superior to those of torsatrons typically by 50%. (The first results from LHD, presented at this conference, indicate improvements in comparison to the scaling expectation /20/). The separate shear studies on W7-AS do not give evidence that the reason is the difference in shear of the two helical concepts. The τ_E scaling of W7-AS alone is: $\tau_E \approx B^{0.73} P^{-0.54} n_e^{0.5} L^{2.72}$. The size scaling (L) is selected to have correct dimensions. It is close to the size scaling of ISS95: $L^{2.86}$. The data base of W7-AS also shows the saturation of confinement time with ECRH heated plasmas at higher densities when analysed by Bayesian probability theory /21/. The W7-AS scaling can be rephrased in dimensionless parameters: $B\,\tau_E \approx \rho^{-2.53} \beta^{-0.03} \nu^{-0.06}$. The scaling is between Bohm and gyro-Bohm.

In the above mentioned ι-ranges the confinement can be improved above the L-mode level. Similar to the tokamak, two obviously different paths are possible: The first is the establishment of the H-mode edge conditions and the second the steepening of the density profile. Apart from

the insight, that the H-mode is rather universal and not restricted to the conditions of tokamaks, the studies on W7-AS have shown that the H-mode develops in specific ι-ranges where poloidal flow damping (from the field structure) is low /22/.

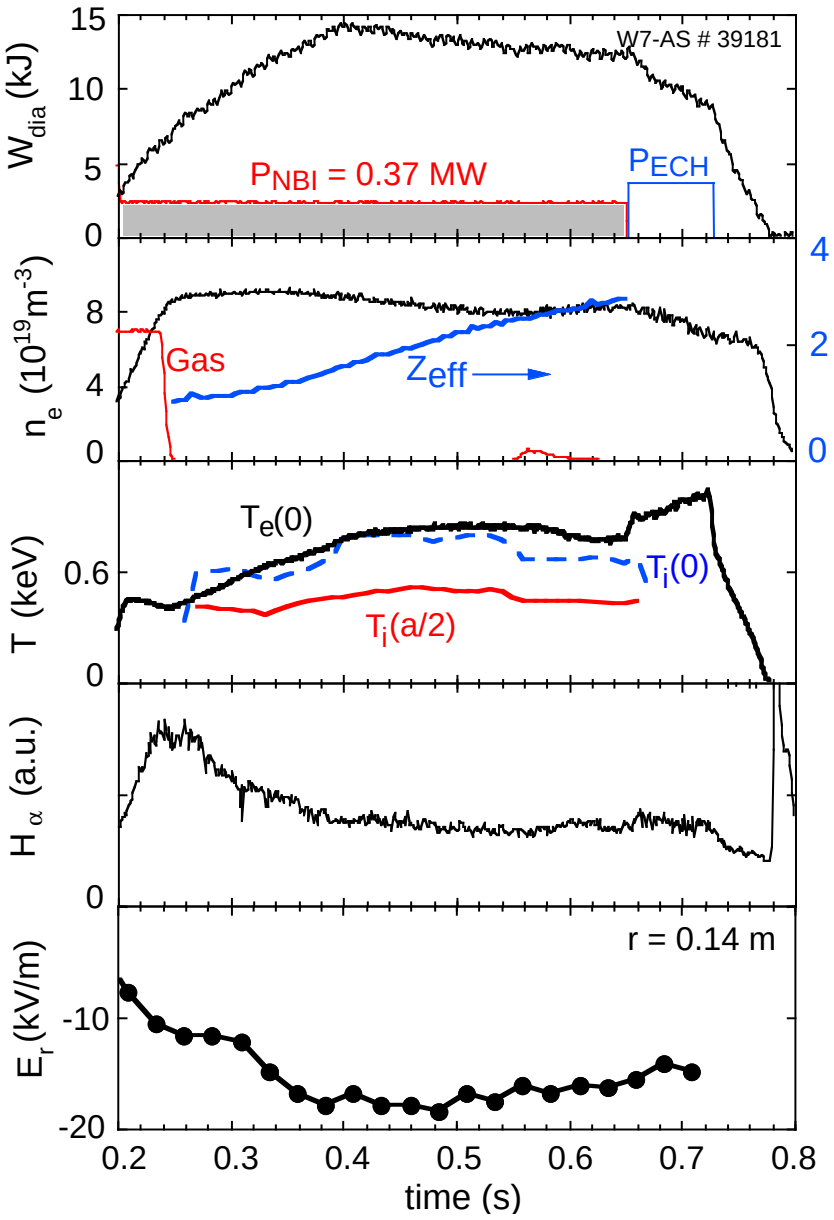

Fig. 4 plots the energy content W_{dia}, the density n_e and Z_{eff}, the temperatures, the H_α radiation and the spectroscopically measured radial electric field E_r versus time for a low power beam heated discharge. At constant density, the confinement improves spontaneously from about 0.25 to 0.4 s.

Figure 4 shows an alternative path to good confinement /30/. The development of the plasma energy content is spontaneous but occurs on a slow time scale ($\delta t \approx \tau_E$). An interesting aspect of this regime is that the energy content rises at constant density via the rise in T_e and T_i. The gradual improvement is accompanied by a gradual reduction of H_α which itself is quiescent. E_r becomes more and more negative and develops along the neoclassical expectation. The major characteristics of this confinement regime is the narrowing of the density profile and low edge density. The technical prerequisite is a well conditioned device with low recycling properties and boronised walls. There is strong reminiscence to improved tokamak regimes which demonstrate a similar link between bulk confinement quality, edge properties, recycling control and density profile development /23/. The source fuelling by NBI or combined NBI+ECRH contributes to the

profile peaking. In the initial phase of confinement improvement, the T_e profile gradually expands. At low power (0.5 MW) and high density (10^{20} m^{-3}), τ_E values above 50 ms have been observed - a factor two above ISS95 and in the ball park of expectations based on ELMy H-mode scaling.

Particle transport:

Stellarator density profiles are flat in the plasma core under central heating conditions without central fuelling. The gradients reside at the plasma edge in the range of the recycling source. With core fuelling (NBI), profiles peak as a consequence of the changed source distribution. With strong central ECRH, the density profile becomes even hollow. With off-axis ECRH heating and flat central temperature profiles, the core density profile peakens (see Fig. 5) /24/. EIRENE calculations show that core fuelling is not dominant under the conditions of these experiments.

These observations elucidate the effects which govern the particle transport. Besides diffusion, thermal diffusion plays a role. The experimental analysis shows, that the thermally driven ($\Gamma \propto T_e'$) neoclassical flux component, which is outward directed in stellarators can explain the hollow profiles of central heating. The consequence of this term in particle transport is detrimental because it may lead to unfavourable and even unstable density profiles in larger devices /25/. As a consequence, the existence of a concective inward flow (by the E_r/T-term or resulting from the background turbulence) superimposed onto the other two mechanism has also an important practical aspect. This term in the transport equation was therefore carefully studied in perturbation experiments analysing gas oscillation experiments /26/ and by studying the peaking of the core density profile when ECRH was switched from central to off-axis heating /24/ (see Fig. 5). The modelling of the temporal phases yields an inward velocity of about 1 m/s for the inner half which rises to the plasma edge to about 4 m/s. Though the particle fluxes in the core are generally close to the neoclassical level and 3D-effects of neoclassical transport causes outward directed thermal diffusion, there remains a favourable inward flow term. Nevertheless, particle transport studies and core fuelling techniques will further require specific attention in large helical devices.

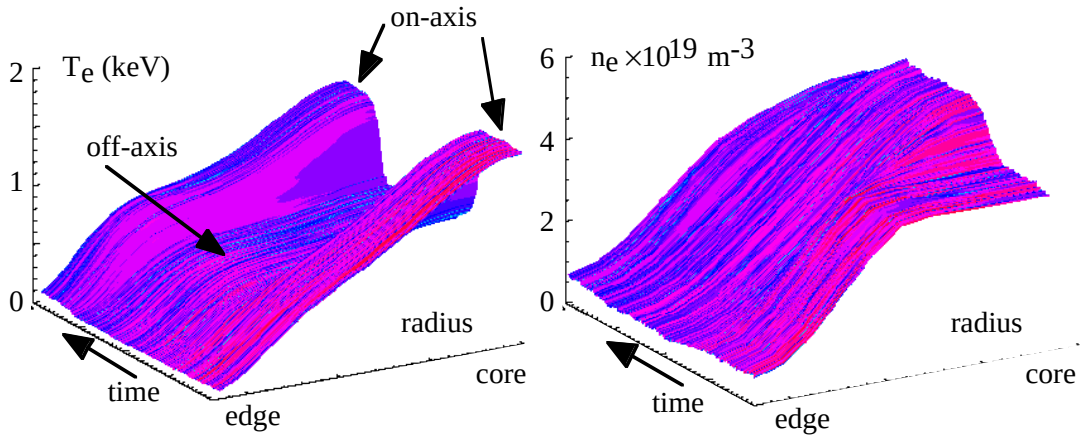

Fig. 5. On the left side, the electron temperature profile (ECE) and on the right side the density profile (10 channel interferometer) are plotted for an experimental scenario, where the ECRH power deposition was varied in steps from the core to the periphery and back again (see arrows).

Impurity transport has been studied by means of different impurity injection techniques like laser blow-off and gas oscillation. For ECRH plasmas with central electron densities of 0.4 - 5 × 10^{19} m^{-3} the radiation decay time of the highest ionization states of laser blow-off injected aluminium (Al XII, Al XIII) - a measure of the global impurity confinement time - scales as

$\tau_{Al} \sim P_{ECF}^{-0.8} n_{eo}^{1.2}$ (ECRH heating power P_{ECF}, central electron density n_{eo}) /27/. The scaling is supported by local transport coefficients (diffusion coefficient D, convective velocity v) obtained from the analysis of radial and temporal soft-X ray profile developments after impurity injection /28, 29/. Typically for ECRH discharges, a moderate diffusion coefficient is observed in the central region ($D \approx 0.2$ - 1 m^2/s, decreasing with density), whereas smaller diffusion coefficients ($D \approx 0.03$ - 0.1 m^2/s) are obtained for the outer third of the plasma.

In low and medium electron density plasmas ($< 4 \times 10^{19}$ m^{-3}) impurity radiation saturates and stationary conditions are achieved during the discharge pulse (typically one second). Towards higher electron densities ($> 5 \times 10^{19}$ m^{-3}) impurity radiation and Z_{eff} often do not reach stationarity within the discharge duration but show a steady increase with the tendency to saturate at times longer than the performed pulse length. Assuming constant impurity sources this behaviour is a consequence of rather low diffusion coefficients as derived from measured data in particular in the outer region of the plasma. These discharges are also expected from modelling to reach a final intrinsic impurity concentration level related to the strength of its source.

A slow increase of Z_{eff} during the pulse duration was also observed in high confinement NBI discharges /30/ (see Fig. 4) at high central electron density (1.2×10^{20} m^{-3}) and a slightly peaked electron density profile. A rather low diffusion coefficient $D(r)=0.07 m^2/s$ and an inward convection velocity of 5r/a m/s were derived from aluminium injection experiments. The implications of the low diffusion coefficients on high density operation will be discussed further below and will be critically assessed in the planned island divertor programme of W7-AS.

Edge transport and turbulence:

Detailed edge transport studies were carried out in W7-AS under limiter conditions (to simplify the analysis) /31/. The dominant scaling parameter is the density both for D and $\chi_e \propto 1/n_e$. With increasing heating power the diffusivities increase and thus reflect the scaling of the global confinement times. It is interesting that the edge transport scales similarly to the global confinement and can, on the other hand, be quantitatively investigated by probes.

In the scrape-off layer (SOL) and around the last closed magnetic surface (LCMS), arrays of Langmuir probes are used to investigate the spatio-temporal structure of ion saturation current (I_{sat}) and floating potential (Φ_{fl}) fluctuations and to determine the radial flux. Density fluctuations can be observed from the SOL to several cm inside the LCMS with a fast Li beam diagnostic by applying a deconvolution technique to the radial correlation function of the Li light profiles /32/. For the SOL, the fluctuation characteristics from these measurements are in agreement with those found by Langmuir probe measurements and rule out major falsifications of the data caused by the probe.

These fluctuations exhibit broad spectra decaying rapidly towards high frequencies. Most of the spectral power is located below a few 10 kHz. A characterisation in terms of correlation functions shows typical lifetimes of 10–30 μs, poloidal correlation lengths of few cm and radial correlation lengths about half the poloidal correlation lengths (i. e. of the order of the radial gradient scale lengths) /33, 34, 40/. Parallel to the magnetic field, a correlation of 90% for 6 m distance between probe tips has been found in the SOL both for I_{sat} and Φ_{fl} /34/. The fluctuations thus have the character of filaments extending between the intersections of a magnetic flux bundle with the limiters. These structures are moving poloidally with several 100 m/s (at 2.5 T) up to 2000–4000 m/s (at 1.25 T) in the ion diamagnetic drift direction in the SOL and in the opposite direction inside the LCMS. Just inside the LCMS, the correlation parallel to the magnetic field is found to be 40–50% for a probe separation of 32 m /35/. Whether this reduction in the parallel correlation is due to the different magnetic field topology on closed magnetic surfaces, due to the higher distance between the probes or due to the fact that the stabilising impact of the high field side enters (in contrast to the SOL measurements), remains to be investigated. I_{sat} and Φ_{fl} fluctuations are well correlated, with a phase angle of $\pi/4$-$\pi/2$, resulting in an outward directed

net particle transport dominated by few short and poloidally located „events" /34/. The spatial and temporal scales of the fluctuations in the SOL, their amplitude and the induced radial transport are well reproduced by a two-dimensional drift-interchange code which allows for a self-consistent development of the radial profiles and retains the sheath boundary conditions at the limiters /37/.

The technique of fast swept Langmuir probes was used to measure simultaneously plasma density, electron temperature and plasma potential fluctuations /38/. For those discharge conditions used, T_e fluctuations have a somewhat smaller relative fluctuation amplitude than density fluctuations ($\tilde{T}_e/T_e \approx 0.5\,\tilde{n}_e/n_e$) and the fluctuations of these two quantities are almost in phase. The conductive part of the radial electron energy transport due to fluctuations of the radial E×B velocity is found to be of the same order of magnitude as the convective part: $n<\tilde{T}_e\,\tilde{E}_\theta>/B \approx T_e<\tilde{n}_e\,\tilde{E}_\theta>/B$. It is therefore justified to compare the plasma parameter dependencies of the fluctuation-induced radial particle transport calculated from I_{sat} and Φ_{fl} fluctuations directly with parameter dependencies of the global energy confinement time /39/. The particle transport is reduced and the energy confinement time increases in a corresponding manner when increasing the plasma density, increasing the field or reducing the heating power in ECRH discharges. The confinement variations with n_e, B and P are accompanied by changes in the lifetime and poloidal size of the fluctuation structures. The increases in the radial flux when reducing the density or increasing the heating power are caused by increases of the fluctuation amplitude, predominantly of the potential fluctuations /40/. Details will be published elsewhere.

High density operation:

Stellarators can operate at high density. The limitation is by a breakdown of the energy balance at the plasma edge due to excessive radiation and recycling losses /41/. The plasma decay is slow and can be influenced at any phase by reduction of the gas-flow rate or by increasing of the heating power. Of relevance for larger devices is the scaling of the maximum operation density (the value which can be stably sustained). Both edge and line averaged density scale with power and field. The edge density scaling is: $n_e \approx B^{0.8}\,P^{0.5}\,L^{-0.62}$. The L-scaling is selected to yield a dimensional correct relation. With the heating power foreseen for W7-X, the operational density would surpass the one achieved in W7-AS.

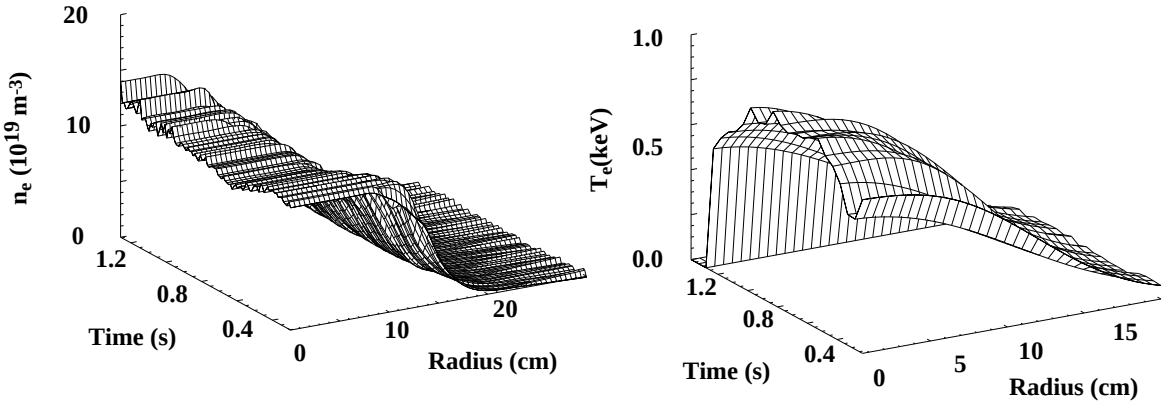

Fig. 6. Time evolution of radial profile of electron temperature and density from Thomson scattering.

The kinetics of the radiative decay of high-density discharges was studies at reduced beam power (380 kW). As there is no MHD stability criterion involved rather the impurity radiation plays a decisive role, the main emphasis is the possible modelling of density limit discharges on the basis of the measured transport coefficients. At B = 2.5 T, beam fuelled discharges were

established with constant central densities from 1.1×10^{20} m^{-3} to 1.6×10^{20} m^{-3}; during each density plateau a peak in the diamagnetic energy developed and the level of radiated power rose during the discharge. The diamagnetic energy decreased faster in the collapse phase at higher density. The magnetic configuration was bounded by the two tangential limiters at the top and bottom of an elliptical cross section for discharges with $\iota(a)$ of 0.34. The radial profiles of the diffusion coefficient, D, and inward pinch velocity, v, were calculated from measurements of the time evolution of soft x-ray emission and Al impurity lines after aluminum impurity injection by laser blow-off /29/ as described above. Using the radial profiles of D and v derived from laser blow off experiments, together with the time evolution of the density and temperature profiles and an assumed constant impurity flux of each impurity at the boundary, simulations of the time evolution of bolometer and soft x-ray radiation profiles were carried out with the transport code ASTRA /42/ and the impurity transport code STRAHL /43/. In Fig. 6, the time evolution of the radial profiles of the electron temperature and density from Thomson scattering are shown. In Fig. 7, the measured and simulated radiation profiles for the bolometer and soft x-ray (12.5 mm beryllium foil filter) cameras for the density plateau discharge considered are compared. These simplified assumptions are sufficient to satisfactorily simulate the peaking of the measured bolometer and soft x-ray profiles and show that during the discharge the impurity density profiles with a central peak continuously increase. Equilibrium is not reached as the time constant for this process is much longer than the duration of the discharge. The consequent increase of the central radiated power and the decrease in net power to the plasma together with the slow central density rise, leads to a reduction of the central temperature which reinforces the increase in radiated power and finally terminates the discharge. These studies are the first step to predictively model the high density operational limit in W7-AS.

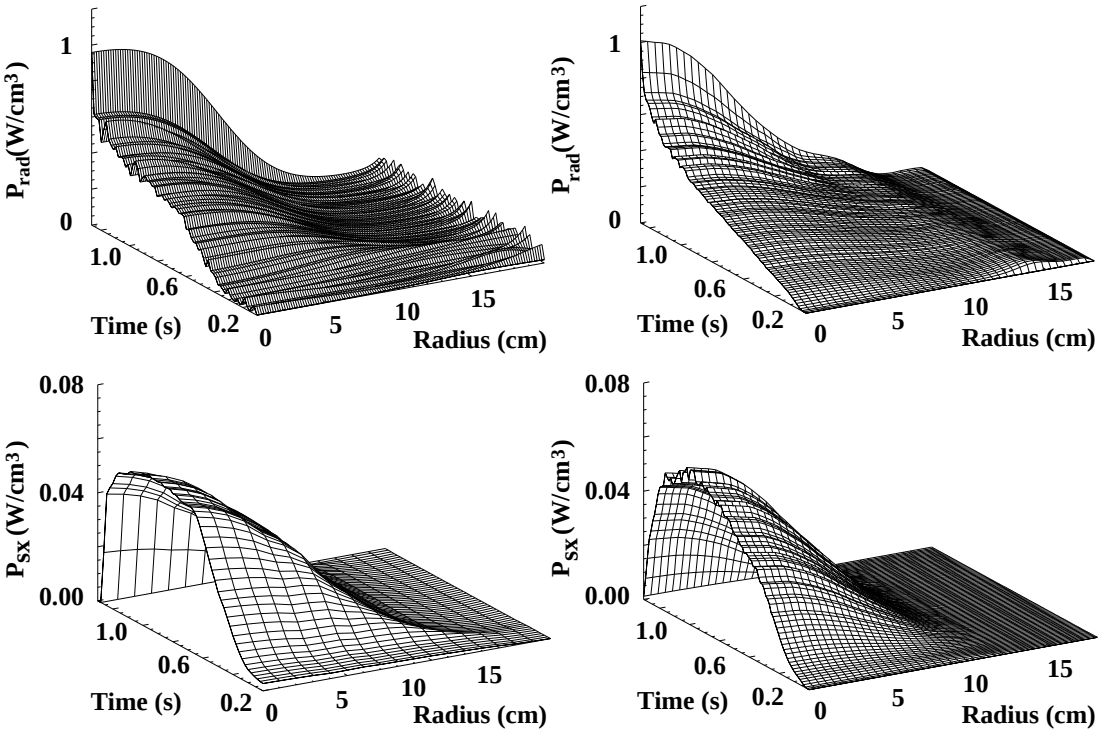

Fig.7. A comparison of the measured (see Fig. 6) and simulated (right column) radiation profiles for the density plateau discharge. The radiation profiles deduced from the bolometer and soft x-ray (12.5 mm Be filter) cameras are shown in the first and second rows respectively. The bolometer and soft x-ray profiles were simulated using a diffusion coefficient and an inward pinch coefficient profile calculated from Al laser blow off experiments and time dependent electron temperature and density profiles with the impurity transport code STRAHL and the time dependent transport code ASTRA. Three impurity flux sources (C, Cl and Cu) at the plasma boundary were assumed.

The island divertor concept:

W7-X will be equipped with an island divertor /44/. W7-AS already allows basic elements of this concept to be evaluated. At $\iota(a) > 0.4$, the edge is bounded by a chain of intrinsic 5/m magnetic islands (with m = 8, 9, 10 in the W7-AS case). The device is presently operated with poloidal inboard limiters which, however, will be replaced in 1999 by ten symmetrically arranged island divertor modules (designed for 5/9 boundary islands) with strong geometrical similarity to the W7-X divertor concept /45/. The divertor concept was prepared by experiments on the plasma flow diversion by islands /46/ and by predictive code simulations of island divertor scenarios. A 3D edge transport code EMC3 (Edge Monte Carlo 3D) has been developed /47/, coupled to the EIRENE neutral transport code /48/, and first applied to pure hydrogen plasmas (inclusion of impurity transport is under way) in the 5/9 island divertor configuration. In parallel, the (geometrically less adequate) B2-EIRENE code /49/ was applied to the same, but helically averaged configuration /50/ for „proof of principle“ predictions including more complete physics (impurity transport, strongly radiative and detached scenarios), and for benchmarking the EMC3-EIRENE code. The EMC3-EIRENE code is a candidate also for future W7-X applications.

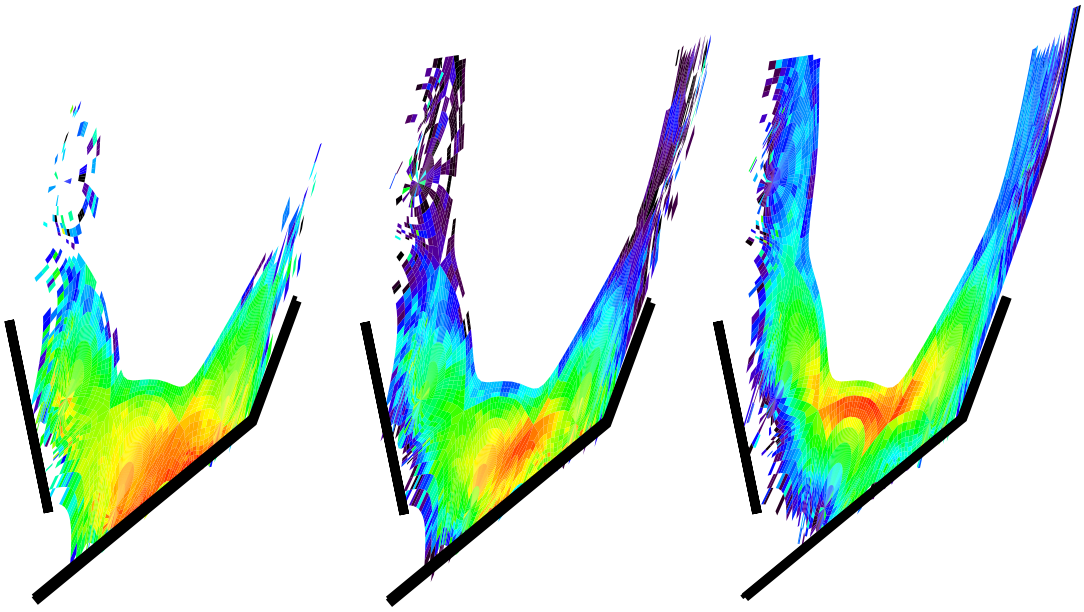

Fig. 8. Shown is a half-cross section of the W7-AS plasma near the elliptical plane; the planned divertor structures (target and baffles) as sketched. Plotted is the ion source for three different density values. Density increases from left to right.

The results of these preliminary studies show gross agreement with tokamak x-point divertor scenarios, but in detail reflect characteristic geometrical differences. In contrast to tokamak divertors, island divertors in stellarators necessarily have a 3D magnetic structure, toroidally discontinuous targets (localised recycling zones), smaller radial separations between target and main plasma, and, in general, longer field line connection lengths from target to target (small field line pitch inside the islands). These features affect the penetration of recycling neutrals and impurities into the main plasma, as well as the ratio of the cross-field to parallel transport (plasma flow diversion) within the SOL. Both are crucial for divertor performance. Nevertheless, the experiments mentioned give strong indications of a significant radial diversion of the plasma flow by the islands even at these conditions /45/. Slight asymmetries of the plasma flow measured inside the islands at low density, could be well reproduced by the EMC3-EIRENE code by superimposing an E×B plasma drift caused by T_e profiles decreasing towards the O-point /51/. With increasing density and for typical heating powers and cross field transport coefficients /31/, the code results predict edge parameter regimes passing through the same sequence as in tokamak divertors: from a linear SOL regime over high recycling with strong particle flux

enhancement (both, EMC3-EIRENE and B2-EIRENE) to stable (energy) detachment with strong divertor radiation and very low divertor leakage for neutrals (B2-EIRENE, multifluid, with carbon sputtered from the targets). Figure 8 shows the ion source $n_e n_0 \langle \sigma v \rangle_{ion}$ for various densities. At high density (right side), the ionisation front has moved away from the target plate to the separatrix. The stability limit coincides with a breakdown of the particle flux to the targets (complete detachment). In contrast to typical tokamak scenarios, the stronger contributions from cross-field transport of energy, particle and momentum lead to significantly flattened downstream deposition profiles over the whole density range and to „layer"-type detachment. Diffusive and viscous radial coupling of particles flowing in opposite direction along the closely neighboured island fans is found to cause momentum losses for the single fans in addition to charge exchange losses thus easing the transition to detachment. Varying the field line pitch by factors of 1/2 - 2 (by special control coils in W7-AS) does not substantially change this picture.

Wave heating:

The accessible plasma density for ECRH with electromagnetic waves in ordinary and extraordinary polarisation (O- and X-mode) is limited by plasma cut-off. For the electrostatic electron Bernstein wave (EBW), the third EC-mode which is able to propagate in a hot plasma, no such limit exists. However, since EBWs cannot be excited from the outside, they have to be generated via mode conversion from the electromagnetic waves. One possible way for this is the so called OXB-process /52/. In a first step (OX-process) a slow ($v_{ph} < c$) X-wave is generated at the O-mode cut-off density from a fast ($v_{ph} > c$) O-wave launched from the outside with an optimal angle oblique to the magnetic field vector. The X-wave then propagates towards the upper hybrid resonance (UHR) layer, where it is converted into an EBW (XB-process). Both processes take place at the density gradient region and are very sensitive to the plasma conditions there (level of turbulence). The influence of the plasma parameters on the conversion efficiencies was investigated at W7-AS for 70 GHz ECRH-frequency. For both processes optimal target plasma conditions could be found, so that the EBWs were generated with an efficiency of more than 80%. After the OXB-process the EBWs propagate towards the dense plasma centre, where they are absorbed near the cyclotron resonance layer. The radial absorption profile was estimated from the soft X-ray emission by switching the power. The radial shift of the absorption zone was investigated by changing the position of the ECR-layer in a magnetic field scan. Due to the very strong damping of the EBWs and due to a non vanishing parallel component of the EBW vector (oblique launch), a large Doppler shift of the EC-absorption towards the lower field is seen. For our experimental plasma parameters (T_e=500 eV, $n_e = 1.5 \times 10^{20}$ m^{-3}) central EBW-heating could be achieved for a central magnetic field of 2.13 T. The target plasma was sustained by 360 kW NBI. Additional OXB-heating with a power of 330 kW increases the plasma energy as well the central plasma temperature by 30% (ΔW=2.5 kJ, ΔT=110 eV) compared with a discharge with NBI only.

Also the inverse process, the EB-wave emission through the O-X-B angular window was detected and EB-wave emission spectra were measured. Beside the local thermal cyclotron emission of EB-waves, which in principle could then be used for temperature measurement, nonlocal broad-band EB-radiation was found /53/.

Operation of ICRH from the high-field-side with a narrow $k_{||}$ spectrum successful ICRF heating became possible /54/. In resonant and non-resonant heating scenarios, the ion and electron temperature of ECRH and NBI target plasmas were increased. Simultaneously the plasma density could be kept constant and there was no rise in impurity concentration. The investigated scenarios were: D(H), ^{4}He(H) minority heating (minority species in brackets), D/H mode conversion heating, second harmonic H heating. Since recycling strongly determines the plasma composition, proper wall conditioning was imperative to obtain sufficiently low hydrogen concentration for minority heating. The efficiency of these scenarios was determined by comparing the increase in diamagnetic energy with expectations based on power scaling. Thus the

efficiency was found to be comparable to that obtained in tokamaks. In particular, D(H) minority heating is similarly more efficient than second harmonic hydrogen heating. Using the same heating scenarios it was also possible to sustain target plasmas solely with ICRF. Several energy confinement times into the ICRF phase, the plasma parameters reached steady-state values of density, temperatures and impurity radiation. The duration of these discharges was determined only by arcs in the RF system or limited on purpose to avoid excessive ohmic heating of the uncooled antenna. The maximum plasma duration was one second.

References

/1/ NÜHRENBERG, J., et al., Trans. Fusion Technology, 27 (1995) 71
GORI, S., et al., in Theory of Fusion Plasmas, 1996, 335
LOTZ, W., et al., in Plasma Physics and Controlled Nuclear Fusion Research 1990 (Proc. 13th Int. Conf. Washington, 1990) Vol.2, IAEA, Vienna (1991) 603
WOBIG, H., Plasma Physics and Controlled Fusion 33 (1993) 687
/2/ SAPPER, J. et al., Fusion Technol. 17 (1990) 62
/3/ RENNER, H. et al., Controlled Fusion and Plasma Physics, Proc. 19th European Conf. (Innsbruck, 1992) Vol 16C pt I, p 501.
/4/ GRIEGER, G., et al., Phys. Fluids B 4 (1992) 2081.
/5/ GEIGER, J., et al., Proc. 23th EPS Conf. on Contr. Fusion. and Plasma Physics (Kiev) 20C Part II, 491 (1996)
/6/ PENNINGSFELD, F.P., et al., Proc. 23th EPS Conf. on Contr. Fusion. and Plasma Physics (Kiev) 20C Part II, 483 (1996)
/7/ KICK, M., et al., in Plasma Physics and Controlled Nuclear Fusion Research 1996 (Proc. 16th Int. Conf. Montreal, 1996) Vol.2, IAEA, Vienna (1997) 27
/8/ ERCKMANN, V., this conference
/9/ WAGNER, F., et al., Proc. 25th Eur. Conf. on Controlled Fusion and Plasma Physics Prague, 1998, to be published
/10/ WELLER, A., this conference
/11/ NÜHRENBERG, C., submitted to Phys. Plasmas
/12/ SPONG, D.A., et al., Nucl. Fusion 35 (1995) 1687
/13/ BRAKEL, R., et al., Plasma Phys. Contr. Fusion, 39B, 273 (1997)
/14/ BRAKEL, R., et al., J. Plasma and Fusion Res. SERIES, 1, 80 (1998)
/15/ BRAKEL, R., Proc. 25th Eur. Conf. on Controlled Fusion and Plasma Physics Prague, 1998, to be published
/16/ KICK, M., 25th Eur. Conf. on Controlled Fusion and Plasma Physics Prague, 1998, to be published in Plasma Phys. Contr. Fusion.
/17/ MAASSBERG, H., et al., submitted for publication in Plasma Phys. Contr. Fusion
/18/ MAASSBERG, H., et al., submitted for publication in Plasma Phys. Contr. Fusion
/19/ STROTH, U., et al., Nucl. Fusion 36(8) (1996)1063
/20/ IIYOSHI, A., this conference
/21/ DOSE, V., et al., accepted for Phys. Rev. Letters
/22/ HIRSCH, M., et al., in Plasma Physics and Controlled Nuclear Fusion Research 1996 (Proc. 16th Int. Conf. Montreal, 1996) Vol.2, IAEA, Vienna (1997) 315
/23/ WAGNER, F., et al., Plasma Phys. Contr. Fusion 35, 1321, 1993
/24/ STROTH, U., et al., submitted to Phys. Rev. Letter.
/25/ SIMMET, E.E., et al., Proc. of the 24th Europ. Conf. on Controlled Fusion and Plasma Physics, Berchtesgaden, 1997, Vol. 4, p. 1673.
/26/ KOPONEN, J.P.T., et al., to be published in Nucl. Fus.
/27/ BURHENN, R., et al., Proc. 22nd EPS Conf. on Contr. Fusion. and Plasma Physics (Bournemouth) 19C Part III, 145 (1995)
/28/ BURHENN, R., et.al., Rev. Sci. Instrum., Vol.70, No. 1, (1999), (to be published)
/29/ BURHENN, R., et al., Proc. 24nd EPS Conf. on Contr. Fusion. and Plasma Physics (Berchtesgaden) 21A Part IV, 1609 (1997)
/30/ STROTH, U., et al., Plasma Phys. Control. Fusion 40, 1551 (1998)
/31/ GRIGULL, P., et al., Proc. 10th Intern. Conf. on Stellarators, IAEA Technical Meeting, Madrid, Spain, 1995, Report EUR-CIEMAT 30 (1995), p. 73

/32/ ZOLETNIK, S., et al., Plasma Phys. Contr. Fusion 40 (1998) 1399-1416
/33/ BALBÍN, R., et al., 19th EPS Conf. Contr. Fus. Plasma Phys. (Innsbruck), 16C, part II (1992), 783-786
/34/ ENDLER, M., et al., Physica Scripta 51 (1995), 610-616
/35/ BLEUEL, J., et al., 24th EPS Conf. Contr. Fus. Plasma Phys. (Berchtesgaden), vol. 21A, part IV (1997), 1613-1616
/36/ BLEUEL, J., et al., 23rd EPS Conf. Contr. Fus. Plasma Phys. (Kiev), vol. 20C, part II (1996), 727-730
/37/ BLEUEL, J., et al., 25th EPS Conf. Contr. Fus. Plasma Phys. (Prague, 1998)
/38/ GIANNONE, L., et al., Phys. Plasmas 1 (1994), 3614-3621
/39/ PFEIFFER, U., et al., Contrib. Plasma Phys. 38 (1998), 134-144
/40/ BLEUEL, J., Elektrostatische Turbulenz am Plasmarand des Stellarators W7-AS, PhD thesis, Technische Universität München (1998), Max-Planck-Institut für Plasmaphysik Report IPP III/235
/41/ GRIGULL, P., et al., Proc. 11th Int. Stellarator Conf. & 8th Int. TOKI Conf. on Plasma Physics and Controlled Nulear Fusion, Toki, Japan, 1997, J. Plasma Fusion Res. Series, Vol. 1 (1998) 291
/42/ PEREVERZEV, G. et al., IPP Report 5/42, 1991
/43/ BEHRINGER, K., JET Report, JET-R(87) 08, 1987
/44/ KISSLINGER, J., et al., 21th EPS Conf. Contr. Fus. Plasma Phys. (Montpellier), vol. 18B, part I, p. 368
/45/ SARDEI, F., et al., J. Nucl. Mater. 241-243 (1997) 135
/46/ GRIGULL, P., et al., J. Nucl. Mater. 241-243 (1997) 935
/47/ FENG, Y., et al., Proc. 13th Intern. Conf. on Plasma-Surface Interactions, San Diego, USA, 1998, to be published in J. Nucl. Fusion
/48/ REITER, D., The EIRENE Code, Report No. 2599, Institut für Plasmaphysik, Association EURATOM-KFA, Jülich, 1992
/49/ BRAAMS, B.J., A Multi Fluid Code for Simulation of the Edge Plasma in Tokamaks, Report No. (NET) EUR-FU/XII-80/87/68, Comm. of the EC, Brussels, 1987
SCHNEIDER, R., et al., J. Nucl. Mater. 196-198 (1992) 810
/50/ HERRE, G. et al., Proc. 13th Intern. Conf. on Plasma-Surface Interactions, San Diego, USA, 1998, to be published in J. Nucl. Fusion
/51/ FENG, Y., et al., 24th EPS Conf. on Controlled Fusion and Plasma Physics, Berchtesgaden, Germany, 1997, Erophys. Conf. Abstracts 21A, IV, p. 1569
/52/ PREINHAELTER, J., and KOPECKY , V., J. Plasma Phys. 10 (1973) 1
LAQUA, H.P., et al., Phys. Ref. Let. Vol. 78, No.18, pp.3467-3470, 1997
/53/ LAQUA, H.P., et al., Phys. Ref. Let. Vol. 81, No.10, pp.2060-2063, 1998
/54/ HARTMANN, D., this conference